Large-Aperture Ground Terminal for High Data Rate Free-Space Laser Communications

Ashkan Arianpour, Janak Carey, John Gardiner, Mike Serrano, Aaron Sharpe, Tony Truscott, Andrew Doan, Cameryn Yow, Connie Wang, Graham Nelson, Matt Frowiss
Quartus Engineering, Inc. 9689 Towne Centre Drive San Diego, 92131

ABSTRACT

High-data rate satellites capable of communicating with ground-based terminals circumvent the cost and effort required to physically lay networks of communication fiber in rural and metropolitan areas. However, the alternative of free-space laser communication has its own challenges. First, collimated beams incur dynamic pointing and wavefront errors when propagated through atmosphere. Additionally, due to the unknown tilt of the atmosphere during open loop transmissions, an uplink system with a single uplink assembly would suffer from low irradiance at the space terminal requiring the use of multiple independent uplink assemblies. Here we describe a bi-directional ground terminal comprised of four independent uplink telescopes with communication and beacon channels and a downlink telescope with integrated adaptive optics (AO) tracking schemes that maximize throughput for single mode fiber coupling. A 1μrad pointing error at 3.3σ CDF was achieved for simulated disturbances under atmospheric conditions with a Fried parameter of approximately 7cm, a Greenwood frequency of nearly 270 Hz, and a measured mechanical jitter of a gimbaled assembly with an 82cm aperture telescope. Open loop calibration was conducted and verified at full system integration under outdoor conditions with stars by taking multiple data sets in a single night with a target pointing error threshold of 37μrad rms.

Keywords: Free space, laser communications, atmospheric propagation, ground terminal, link budget

1. INTRODUCTION

Nearly half of the Earth's population resides in rural areas without access to the internet, primarily due to lack of infrastructure in the form of fiber networks. The effort required to provide internet access to remote locations drives the need to find an alternative to conventional telecommunication. Orbital satellites with line of sight to bi-directional communication ground terminals can provide data to a multitude of locations while minimizing the required infrastructure development. Additionally, by increasing the carrier frequency to the optical regime, the bandwidth extends into the terahertz spectrum and has the potential to provide data rates greater than several gigabits per second, allowing for greater data rate traffic for a growing population[1].

Free-space laser communications does not come without its disadvantages compared to tradition wireless technology. Multiple ground terminals spread across the globe would be needed to ensure a source of communication is always present due to unpredictable weather conditions. In addition, atmospheric conditions heavily influence the quality of the link due to random and uncontrollable environmental events that cause spatial variations in wavefront for a space-to-ground propagating beam[2]. This is especially true for ground terminals operating in atmospheric conditions with large apertures much greater than the Fried parameter, and where the slew rate exceeds the sidereal rate of the earth[3]. Systems operating in modulation schemes that require uniform spatial coherence benefit from real-time feedback and adaptive correction of the transmitted downlink beam. The bandwidth requirement for the adaptive correction is primarily dependent on the tilt frequency spectrum present in the atmosphere for a given environment[4]. Since the atmosphere's proximity to earth is closer than to a satellite, link loss resulting from atmospheric fade are more prevalent due to the near field effects of the phase variations for space-to-ground transmission. Furthermore, for open loop uplink transmissions that rely on ephemeris data, the initial acquisition of an engagement is subject to the unknown atmospheric tilt prior to downlink transmission. Implementing a separate diverging beacon channel distributes the irradiance over a larger area, alleviating the pointing requirement needed for acquisition without sacrificing the quality of the communication link between systems. Implementing multiple beacons spatially separated by the Fried parameter increases the probability of acquisition by transmitting through different sections of the atmosphere compared to a single

Free-Space Laser Communications XXXVI, edited by Hamid Hemmati, Bryan S. Robinson, Proc. of SPIE Vol. 12877, 128771B
 · 0277-786X · doi: 10.1117/12.3000402

transmission[5]. Such a multifaceted system would be compatible in several environmental conditions that could cover the globe to ensure a quality link could constantly be available.

This paper describes an optical ground terminal capable of transmitting and receiving high data rates via free-space beam propagation through turbulent atmospheric conditions. Section 2 describes each subsystem's optical and mechanical design. Section 3 describes the predicted disturbances that include atmospheric conditions and expected losses due to turbulent environments, and mechanical disturbances during operation. Section 4 reviews the verification of each subsystem and after their assembly. Finally, Section 5 depicts the full integration and concludes the capabilities with the addition of future developments.

2. SYSTEM ARCHITECTURE

2.1 Background

The Optical Ground Element (OGE) is primarily comprised of two independent subsystems. The Downlink Optical Assembly (DOA) consists of a telescope, gimbal, cable carrier, and optical bench, and is responsible for actively coupling light into a fiber. The Uplink Optical Assembly (UOA) includes optical benches that expand and transmit both the uplink and beacon beams while simultaneous tracking the downlink signal. There are four UOAs operating independently with four beacon channels to increase the probability of engaging with a satellite during open loop acquisition. Automated beam control and guidance is integrated at the subsystem level, while overall software control is implemented at the integrated OGE level.

2.2 Downlink Optical Assembly (DOA)

An altazimuth astronomical telescope design was selected as the base structural architecture of the downlink optical assembly and retrofitted to meet the needs of orbital engagements ranging from Low Earth Orbit (LEO) to Geosynchronous Earth Orbit (GEO). The metallic azimuth support rollers were replaced with paired sets of nylon to reduce the mechanical jitter disturbance driven into the telescope structure. Second encoder position read heads were incorporated into the azimuth and elevation axis positioners to compensate for encoder and bearing eccentricity. A motorized secondary mount is used to account for focus changes of the telescope across varied ambient conditions. A Ritchey-Chretien telescope with 82cm primary mirror comprises the optical prescription with an effective focal length of 5m. The secondary mirror diameter was minimized to reduce the primary mirror obscuration to 4.5% by area. A nasmyth flat mirror folds the beam 90° through the elevation axis of the telescope and into the optical bench for tracking, wavefront correction, and fiber coupling.

The optical bench redirects the downlink beam from the telescope towards three distinct paths: a guidance camera for tracking, a wavefront sensor for measurement of spatial phase coherence, and a fiber for data transmission (Figure 1). A non-common path for downlink, referred to as the calibration path, provides intermittent system checks prior to engagements, but does not affect the downlink signal. The optical bench design provides structural stability from -15 °C to +40 °C, with an "egg-crated" carbon fiber-reinforced bench, inlayed stainless plugs, and invar optical mounts. Angular feedback and tilt correction of the downlink signal is determined using a commercial high framerate CMOS camera array, and an FSM up stream with position feedback based on centroid movement on the guidance camera. The deformable mirror is a Boston Micromachines gold coated piezo actuated continuous mirror with feedback control developed by GuideStar Optical Systems, consisting of a wavefront sensor scaled to match a 50mm sub-aperture at the primary mirror.

Power into the fiber is dependent on the feedback control of the guidance path for maintaining accurate pointing and coupling during an engagement. The annular beam apodization resulting from the secondary's obscuration propagates through the system resulting in a loss in fiber coupling due to mode mismatching with the single mode receive optical fiber. An optical simulation in ZEMAX quantified the maximum fiber coupling efficiency to be approximately 73% with single mode fiber receiving a uniform and diffraction limited beam for the designed telescope obscuration ratio. Figure 1 illustrates the sensitivity to pointing due to the DOA's end-to-end effective focal length being 15m. A pointing error of 1μrad corresponds to approximately -2.6dB of loss when compared to the theoretical maximum for our acceptance aperture.

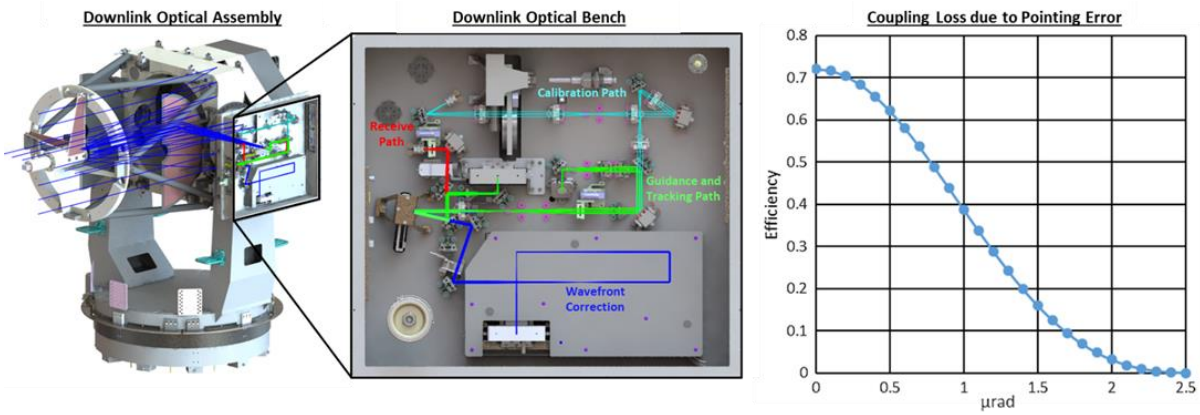

Figure 1. Left) Mechanical CAD and ray trace of the 82cm aperture telescope assembly, Middle) Layout of the downlink optical bench and designated paths, Right) Simulated fiber coupling measurement as a function of pointing error based on receiving a uniform intensity beam at the telescope.

2.3 Uplink Optical Assembly (UOA)

Open loop acquisition, tracking, and point ahead compensation are all necessary for establishing a link with a satellite. The Uplink Optical Assembly can be distinguished by three distinct optical paths in the UOA to perform the necessary functions: a transmit path to the satellite, a receive path for tracking the satellite via the downlink signal, and a bleed path for measuring the relative alignment between the two (Figure 2). Angular feedback of the uplink's transmission is critical during an engagement since the point ahead angle changes based upon the satellite orbital path with respect to the ground terminal. Two separate FSMs operating independently point ahead and track the satellite simultaneously. The tracking FSM of the UOA acquires and tracks the downlink signal during an engagement based on feedback from a guidance camera similar to that in the DOA.

The point ahead FSM is upstream from the guidance FSM and applies the bias angle for pointing ahead of the satellite based upon the azimuth angle of the telescope which correlates to the range and angular rate of the satellite based on feedback through the bleed path. The bleed path consists of an off-90° retroreflector where the center of the six spots represents the pointing direction of the transmit. This allows for the receive and transmit to be co-boresighted to one another without overlapping the beams on the guidance camera. Each UOA has two distinct sources at separate wavelengths: Uplink (data transmission) in C-band near 1550nm and Beacon at L-band near 1600nm. The separate beacon fiber-source rests on an active stage that adjusts position to change the divergence angle at the output space, spreading the irradiance over a larger area at the satellite's location. The total transmitted power of the UOA is near 20W and 10W for Uplink and Beacon, respectively. These power densities are typically high in single mode fiber. However, each of the fibers contain an endcap of fused silica, which cause the beam to enlarge prior to encountering the dielectric-to-air interface thus preserving the structural integrity of the fiber while maintaining a single mode. Having four separated UOAs with beacon channels adds redundancy against atmospheric disturbances during an open loop engagement compared to only utilizing a single UOA with a beacon channel.

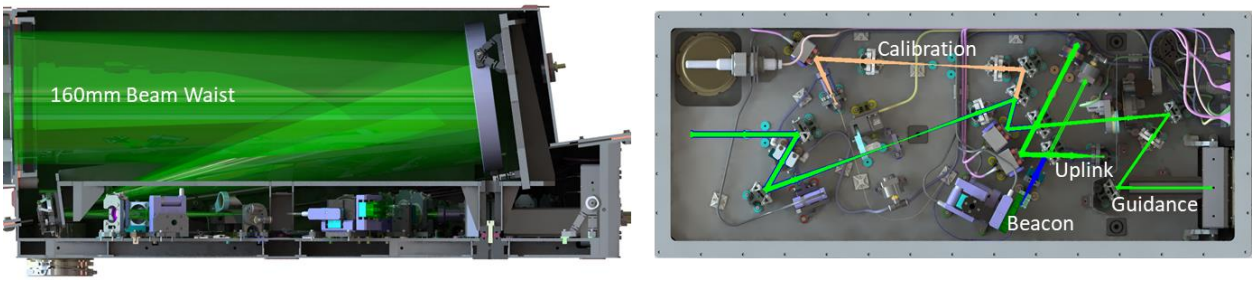

Figure 2. Top) Cross-sectional side view of mechanical CAD and ray trace of off-axis telescope assembly, Bottom) Cross-sectional top view of mechanical CAD and ray trace of uplink optical bench.

3. DISTURBANCE

3.1 Atmospheric Conditions

Atmospheric turbulence dictates the random phase distortions in the wavefront for a beam propagating from space-to-ground, and vice versa. As described in Tyler, pockets of air with varying densities mix due to thermal gradients and results in time-varying optical path lengths[4]. While the position of GEO satellites appears relatively stationary with respect to an observer on earth, satellites in low earth orbit change position rapidly in the sky. Different sites around the globe can be evaluated for their seeing conditions to select the optimal location for a ground terminal. A review of mountainous regions in North America revealed Fried parameters near 7cm under intense atmospheric conditions[6]. This parameter represents a static environment where the beam propagates through a single column of air. When a satellite passes across the sky, the volume of atmosphere that the downlink beam propagates through changes continuously, which can be defined from the ground terminal's perspective as its slew rate. For our system, we define the upper bound of the Greenwood frequency to be 270Hz, representative of a Low Earth Orbit satellite. In addition to changes in wavefront error, which defines the structure of the propagating beam, the slope of the wavefront is approximated as its tilt. Synonymous to the adaptive optics that correct for changes in wavefront, a separate mechanism in the form of an FSM is well-suited for correcting for the tilt component of the received beams. For apertures much larger than the Fried parameter, both mechanisms used simultaneously can maximize the Strehl ratio of the incoming beam while maintaining pointing to maximize fiber coupling. The expected magnitude of the received perturbation spectra of tilt content is dependent on the environmental conditions and inversely proportional to the aperture diameter. A numerical simulation for our environmental conditions and aperture diameters predicted tilt spectral densities for both the UOA and DOA (Figure 3). As expected, the UOA's 240mm aperture observes higher magnitude tilts in comparison to the DOA due to less aperture averaging of the incoming beam.

3.2 Mechanical Conditions

In addition to atmospheric disturbances, mechanical jitter resulting from motion of the telescope on its bearings during a pass induces additional pointing error. Accurate measurement of the magnitude and frequency of these disturbances was critical for developing a control filter to correct for the physical motion and ensure adequate tracking of the satellite. As a final assessment of mechanical jitter would not be possible until full system integration, a predictive approach was developed which coupled system structural models with test data to guide and assess the structural design. First, a finite element model (FEM) was generated and correlated to accurately capture the structural resonant frequencies expected during an engagement. Next, interface accelerations were recovered from several mock engagement tests using accelerometers placed at key locations monitoring the magnitude and frequency of vibration over a 2000Hz bandwidth. Mock engagements were prescribed using simulated two-line element (TLE) files with orbital paths ranging from 30° elevation through keyhole. The effective contribution to pointing error for both the UOA and DOA was then assessed using the correlated FEM by applying the measured interface accelerations and monitoring multi-point constraint equations modeled to represent the optical system sensitivities to physical motion.

Whereas the mechanical jitter assessment captured all sources of vibration inherent in the mechanical system itself, it did not include sources of vibration derived from external sources. One of the additional external sources of vibration affecting the telescope's structure was generated by wind as it passes over the structure. To assess wind, a CFD model was used to quantify surface pressures under multiple potential wind conditions. These surface pressures were then scaled by frequency using the Kolmogorov estimation and applied to the structural FEM as random vibration. Predicted pointing error spectral densities were recovered and combined with the overall predicted error from mechanical and atmospheric disturbances. Figure 3 shows pointing error spectral densities for all the expected disturbances with atmosphere dominating the mechanical jitter and wind buffeting. These predicted spectra were used to optimize the control system to maximize the correction and reduce the residual error in the system.

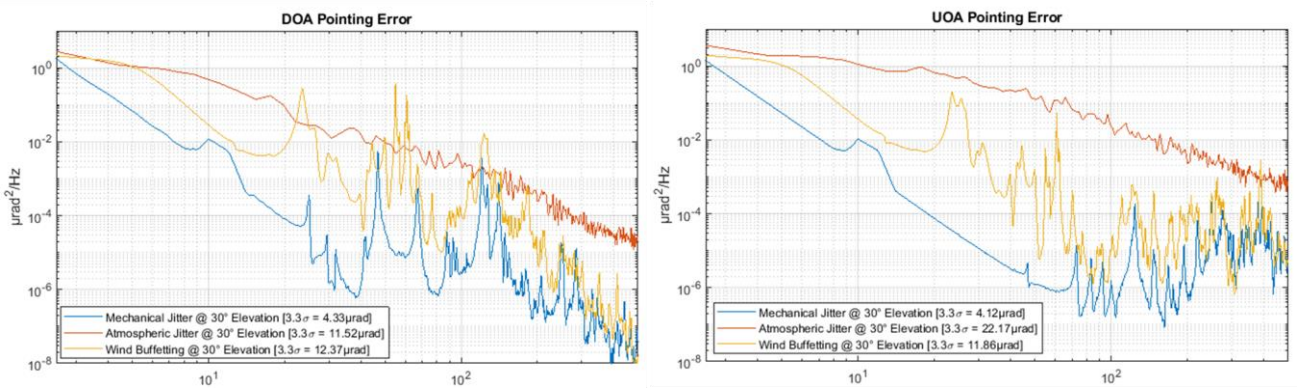

Figure 3. Tilt spectral densities of DOA and UOA for jitter atmospheric, wind jitter, and mechanical jitter.

4. SUBSYSTEM VERIFICATION

Prior to field deployment, system assembly and characterization in a laboratory setting is critical for confirming potential losses during operation. The DOA and UOA were independently aligned and optimized depending on the input disturbance and necessary performance. Subsystems were assembled in a final configuration to verify open loop pointing in an outdoor environment with the available celestial objections.

4.1 DOA Verification

System characterization of the downlink optical assembly is essential for quantifying the expected performance and closing the link at the ground terminal. Misalignment in the DOA consumes stroke in the deformable mirror that would otherwise be used to correct for atmospheric phase accrual. A full aperture interferometric alignment was performed to produce a well-corrected system to alleviate the deformable mirror's allocated stroke for static wavefront correction. For an 82cm aperture, a flat reference mirror would be costly and difficult to mount without affecting the surface figure. Using an 18inch mirror, we stitched several sub-aperture measurements of the telescope (seven sections total), adjusting the secondary after each iteration to reduce wavefront error. The optical bench was independently aligned and mechanically adjusted to be boresighted with the chief ray of the telescope, thereby minimizing precession to be negligible across a 90° slew in elevation. We repeated the previous stitching effort with the integrated optical bench and achieved a peak-to-valley wavefront error of approximately 1110nm, an acceptable loss in deformable mirror stroke.

To quantify the performance of the closed loop control system, we stress tested the vision and FSM loop in a laboratory setting. The calibration path injected a single mode Gaussian beam with an apodization that would theoretically achieve a maximum 78% coupling efficiency. An arbitrary waveform generator applied a transient signal to an external FSM introducing pointing disturbances that replicate the expected self- and wind-induced mechanical jitter, and atmospheric turbulence representing a greenwood frequency of 270Hz with a Fried parameter of 7cm. Fiber coupling was measured simultaneously to verify the results from the guidance camera and control filter. Figure 4 shows tilt spectral densities of the input injection and residual error measured by the guidance camera. The reported pointing error and fiber coupling throughput at 3.3σ was 1.09μrad and 37%, respectively. By measuring the additional transmission losses attributed to cleanliness and coating efficiencies, including the pointing error in relation to the system's theoretical coupling efficiency for the obscuration ratio, the total system loss was determined to be 7dB at 3.3σ. An additional characterization of the DOA verification was conducted by injecting a scintillated beam from a pair of inline rotating phase plates external to the optical bench to verify the closed loop pointing and wavefront correction simultaneously. Both control systems succeeded in correcting for the scintillated input disturbance, replicating the previous pointing accuracy and coupling efficiency into the fiber.

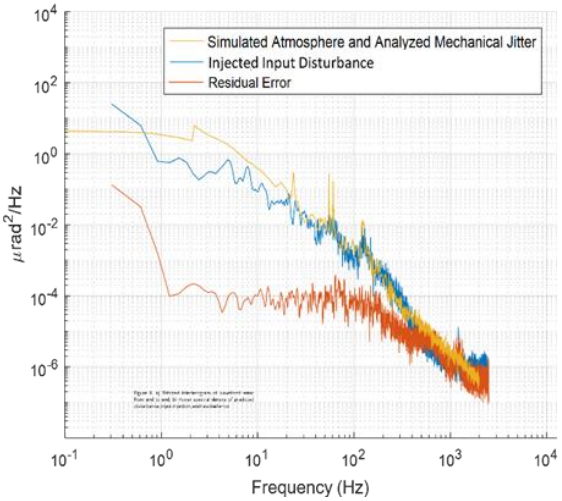

Figure 4. Tilt spectral densities of the DOA for the simulated disturbance, measured input disturbance on guidance camera, and residual error after correction by FSM.

4.2 Uplink

Anisotropy of the atmosphere results in random variations in pointing during closed loop operation. The performance of the uplink optical assembly can be better estimated by modeling the transmission through the anticipated atmospheric conditions and calculating the irradiance distribution over a region of the satellite. To understand the performance criteria required for our wavefront and control system, we performed numerical simulations of multiple Kolmogorov phase screens representing varying altitudes to quantify the expected irradiance distribution at the satellite. The atmosphere simulated consisted of a 7cm Fried parameter and a greenwood frequency of 270Hz for a LEO orbit of 500km. An imperfect wavefront of 100nm of astigmatism and 150nm of defocus were included to envelope assembly tolerances of the as-built system. All simulations included a 3.3μrad offset to reflect the 3.3σ pointing error previously predicted for our control system. Figure 5 shows a single realization of an uplink transmission spanning a region in the sky that is a 60m square. 1 million realizations were evaluated to establish statistical probabilities of various fade depths. A CDF of irradiance vs angle was created to evaluate pointing needs. Figures 5 shows the 1%, 50%, 99%, and 99.9% irradiance cases depending on the pointing error associated with each atmospheric case, and the extrapolated power density for each of the cases.

Four individual UOAs were assembled and characterized prior to integration with the DOA. The measured wavefront error across each of the UOA transmit paths was less than 100nm RMS. The divergence of the transmitted signal in each Uplink channel is influenced by their respective beam waists, each achieving a beam waist diameter of approximately 160mm. The closed loop pointing error was measured similar to the DOA with an external source and FSM injecting disturbances quantified in the previous section. The guidance path FSM corrected the pointing based on feedback from the guiding camera, resulting in a residual pointing error measured to be 5.7μrad at 3.3σ.

4.3 Mount Model

The creation of the open-loop mount model relied on utilizing a series of stars distributed as uniformly and hemispherically as possible. The telescope was initially aligned east to establish a 0° reference direction. A visible camera was mounted to the hub of the telescope with an instantaneous field of view (IFOV) of 12.2μrad. The UOAs and DOA receive light in a narrow band of the infrared spectrum. Stars have a lower radiant intensity in the infrared spectrum compared to the visible spectrum, so a supplemental visible camera can provide more points for the mount model. Five sets of 30 stars were captured and centered on the visible camera with 100 image captures to account for scintillation. Time synchronizing each capture with UTC, and cross referencing with positional data taken from the SIMBAD star catalogue, we could determine the true position of the celestial bodies. With encoder feedback for the azimuth and elevation axes, we quantified the offsets between the expected position and the measured apparent position.

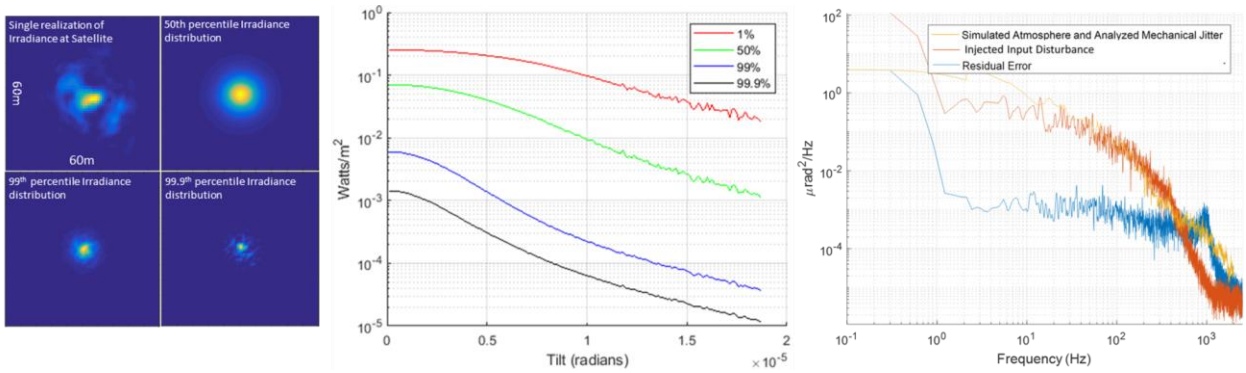

Figure 5. Left) A single realization and 2-dimensional CDFs of 50%, 99%, and 99.9% pointing error through atmosphere (magnitude normalized) of a 160mm uplink beam waist, Middle) Extrapolated power density for each CDF, Right) Tilt spectral densities of the UOA for the simulated disturbance, measured input disturbance on guidance camera, and residual error after correction by the guidance FSM.

The data was then fit to several kinematic and spherical harmonic models. All models resulted in similar calibrations, but ultimately a 9 degree of freedom kinematic model was selected due to the most intuitive, interpretable results. We then confirmed the mount model accuracy from the UOA pointing errors since these systems are ultimately affected by open loop pointing error to begin engagement with the spacecraft. 15 stars were selected for each data set, and five data sets were conducted over the course of the night. An RMS open loop pointing error of 32μrad for the UOA was reported after compiling all five data sets (Figure 6).

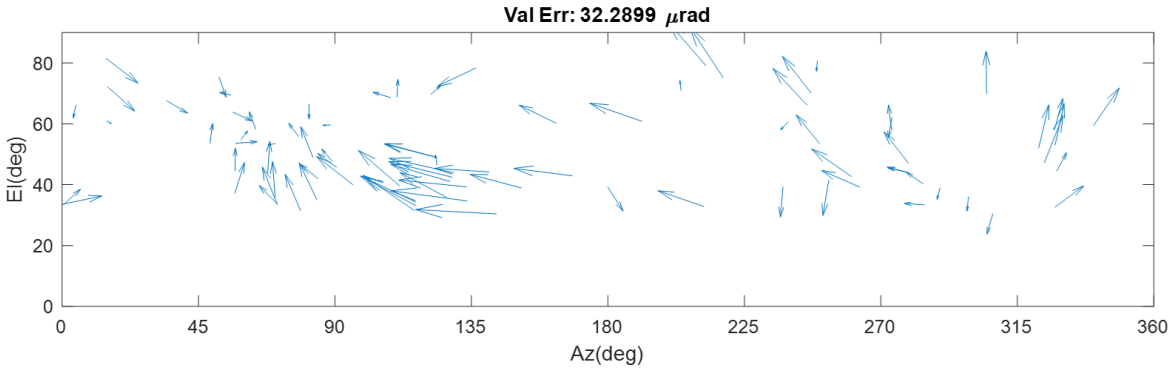

Figure 6. Scaled vector plot of the calibration error of the mount model based on viewing a series of stars.

5. CONCLUSION

After each subsystem verification, the OGE was installed and commissioned in an observatory grade dome. Software and automation features were integrated to reduce operator control. We installed a terrain-based companion terminal with a laser source at distance greater than 10km to emulate the downlink source, filling all apertures of the system simultaneously. Scintillation across the terrain differs from space to ground, however the effects from atmospheric distortion are still present in the form of wavefront and tilt disturbances. Both the tilt and adaptive optic control systems of the DOA successfully closed their respective loops on the companion terminal, correcting for the wavefront distortion and maintaining pointing on the guidance camera (Figure 7). This qualitative demonstration provided assurance for success of the end-to-end performance of the assembled DOA prior to engagement with a satellite.

Relative to a location on the earth, the movement of celestial objects are slow in comparison to a satellite. Previous open loop pointing measurements with stars were not stressed by the synchronicity necessary for a fast-moving target. Without a satellite to measure performance of open loop pointing, we used TLE data to track the ISS based on the star

mount model. Since the ISS is an extended object as seen by our tracking system, we could not engage our guidance system to replicate the tracking performance observed in lab. Furthermore, without knowledge regarding the accuracy of the TLE, we would be unable to precisely quantify the pointing error associated with tracking the ISS. However, with our UOA star-calibrated mount model, we were able to continuously open-loop point at the ISS, capturing its image on the UOA guidance camera near the center of the field of view (Figure 7).

Further testing of the system is ongoing prior to engagement with a satellite. Software and automation are continuously being updated to optimize performance and independence from a human at the controls. Calibration loops are performed intermittently to ensure accuracy of control loops and detect any degradation of system performance. The DOA's and UOA's combination of transmission, wavefront, and pointing losses equated to sufficient margin for our potential engagement. Open loop pointing was measured with stars to be 32μrad RMS. The system has demonstrated compatibility with an expected harsh atmospheric environment and can communicate with space-borne optical payloads for a range of orbits. We are pursuing engagements with on-orbit optical payloads to test the system, and lessons learned from the development will be applied to future endeavors.

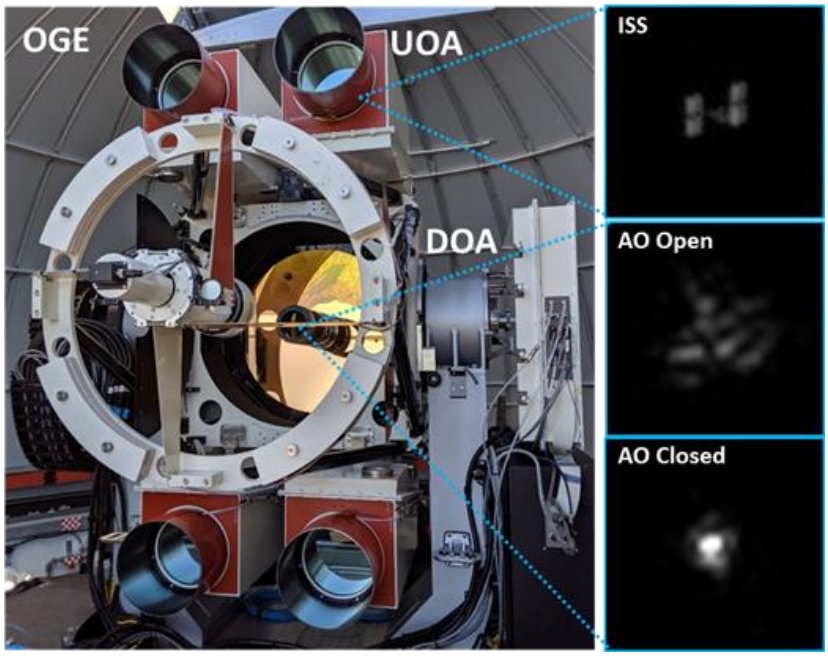

Figure 7. Image of assembled and integrated OGE in a dome, an image of the ISS captured by the UOA in open loop, and images of centroids from the companion terminal during open and closed loop tracking by the DOA.

We would like to thank our collaborators Bart McGuyer, Harvard Harding, Kevin Birnbaum, Chien-Chung Chen, Slaven Moro, Matt Hunwardson, Hamid Hemmati, John Winger, and Donald Link for their relentless support and contributions to the development of this system.

REFERENCES

[1] V. W. S. Chan, "Optical space communications," in IEEE Journal of Selected Topics in Quantum Electronics, Vol. 6, No. 6, 959-975, (2000).
[2] D. Fried and J. Seidman, "Laser-Beam Scintillation in the Atmosphere," J. Opt. Soc. Am. 57, 181-185 (1967).
[3] D. Greenwood, "Bandwidth specification for adaptive optics systems," J. Opt. Soc. Am. 67, 390-393 (1977).
[4] G. Tyler, "Bandwidth considerations for tracking through turbulence," J. Opt. Soc. Am. A 11, 358-367 (1994).
[5] Hemmati, Hamid. Near-Earth Laser Communications. Boca Raton, FL: CRC Press, (2009).
[6] D. Walters, L. Bradford, "Measurements of r0 and θ0: two decades and 18 sites," Appl. Opt. 36, 7876-7886 (1997).